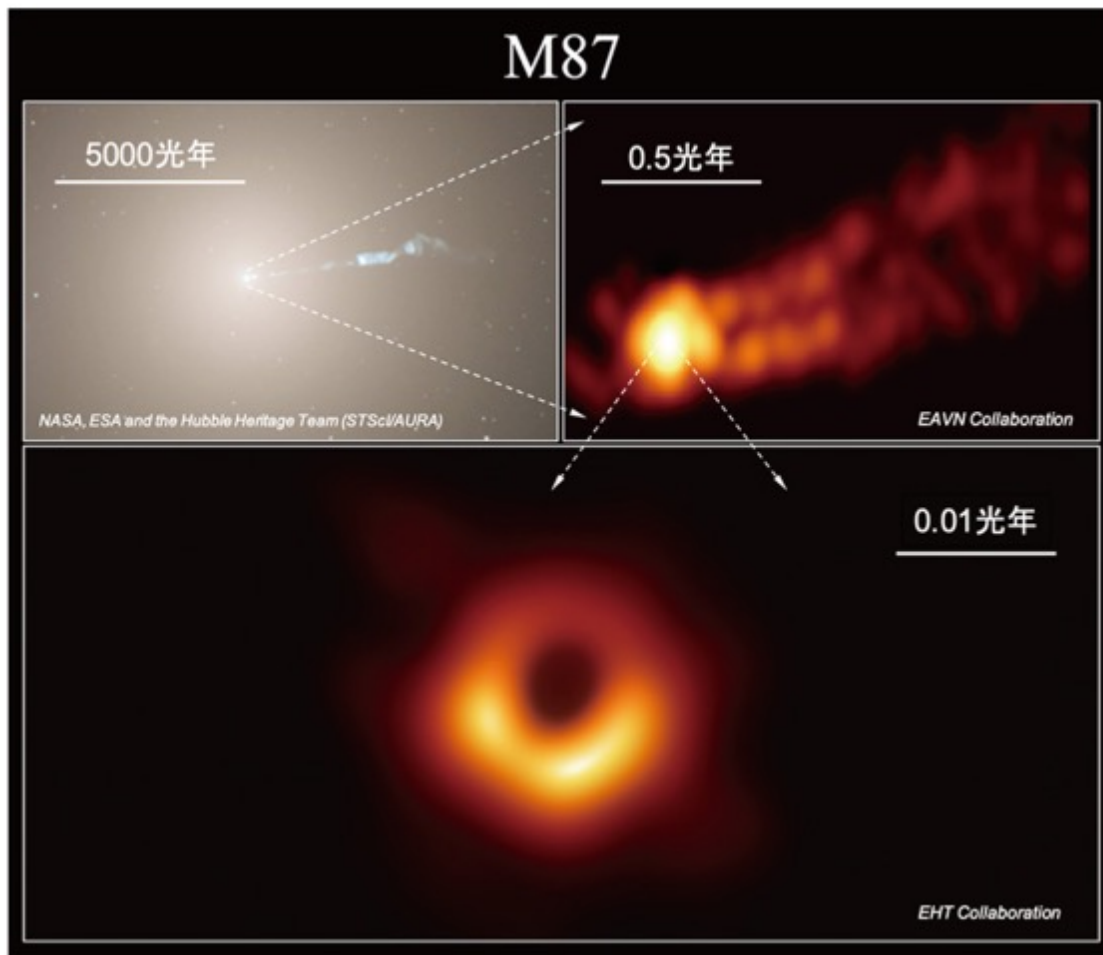


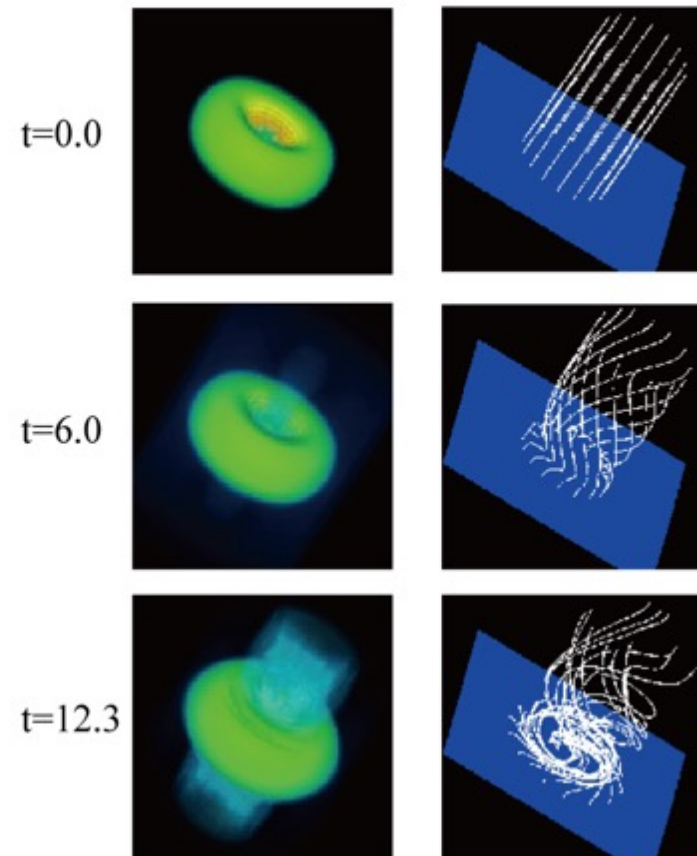
Plasma Astrophysics

Toshiki Tajima, UCI

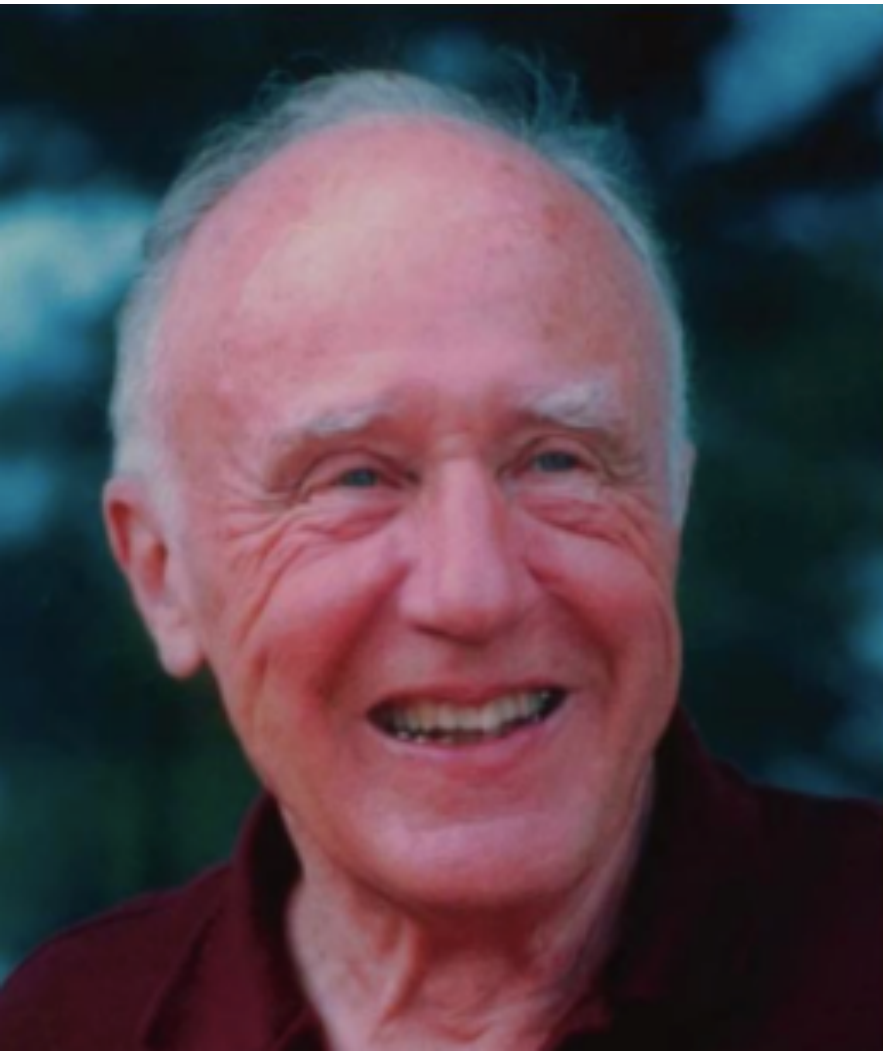
Class 2:PHY249 (2020Spring)



3D Structure of Disk and Jet



John A. Wheeler



*“Toshi, do you know what a professor is about?
A professor is a person who learns from students.”*

Sept., 1980,

Prof. Wheeler at Univ. of Texas at Austin

What part of astrophysics?

- Frontiers of astrophysics only (that are not yet well understood):
 - highest energy particles (e.g. of cosmic rays $> 10^{20}$ eV, high energy neutrinos)
 - highest energy photons (e.g. γ -rays up to TeV /PeV)
 - most violent processes (e.g. disruptive accretion; jets)
 - episodic and eruptive (e. g. γ -ray bursts)
 - young objects (e. g. AGN, Blazars)
 - neutron-star x neutron-star collision \rightarrow plasma plays essential role
 -
- I have no time to cover:
 - old objects (e.g. our galaxy, our Sun, our solar system), gravitational dominants
 - quiet, steady-state objects
 - objects where little plasma such as the Moon (“the older, the less plasma”)
 - single particle interacts with astronomical object (cf. collective interaction N^2)
 -

(our textbook covers some of both kinds)

What can/should we do by the end of the Quarter? (if you are lucky)

- What magnetic fields do in **active Universe**? Why are they there?
- Why **B-fields** important? What do B-fields do?
- What kind of **structure formations**? Accretion disks, jets, collisions of stars (and galaxies),.....
- Survey nonlinear plasma evolution
- What are the Universe's **long standing nonlinear structures**?
- Why **wakefields** are among them and there (does not disappear) and robust?
- Imagine **where** Mother Nature wishes to excite wakefields?
- **Predict** (in addition to interpret) what happens if you make violent plasma excitation?
- Acceleration, emission of gammas, protons, neutrons
- What can you **predict** from all these?
-

Distinction between gravity \leftrightarrow EM

- Both: range can be **infinite** \leftarrow Gauss law
- Strong and weak interactions:
 - \rightarrow range $O(\text{fermi} = \text{fm})$
- Grav: **no** negative mass; EM: + and **-**, but can be combined;
no magnetic monopole \rightarrow magnetic force range finite
- EM: if combined +/- \rightarrow atoms : range $O(\text{\AA})$
- EM: +/- \rightarrow Debye screening: range $O(v_t/\omega_p)$
 - \rightarrow collisionless skindepth: range $O(c/\omega_p)$
 - \rightarrow EM radiation infinite range

However,

- With **B** : fields screening **removed** \leftarrow **Alfven** effect
mediated @ v_A
: **texture** appears
- **Collective**/ violent proc. \rightarrow ephemeral struct. or
 \rightarrow **robust struct = wake** @ c

COSMIC PLASMA

by

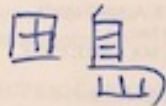
HANNES ALFVÉN

University of California, San Diego, La Jolla, California

and

Royal Institute of Technology, Department of Plasma Physics,
Stockholm, Sweden

To



which thanks for kind help.

阿尔文



D. REIDEL PUBLISHING COMPANY

DORDRECHT · HOLLAND / BOSTON · U.S.A.

LONDON · ENGLAND

Austin 11+3金=月=+3日

Alfven's legacy

Importance of **filaments** / **texture**
in plasma!

ELECTRIC CURRENTS IN SPACE PLASMAS

WITHOUT 'FIELD LINE RECONNECTION' AND 'MERGING' IN THE GNETOSPHERE

ent shows that neither the injection of one test particle, a small s, or all of the solar wind particles call for a change in the magnetic field lines. There is no need for 'frozen-in' field lines moving s for 'field-line reconnection' or 'magnetic merging'. The magnetic atic and not a single field line is 'disconnected' or 'reconnected', d particle is given by Equation (6). There is no 'field-line reconnection' energy to the particles or release energy in any other way. t reconnection models are forwarded by Heikkila (1978). d varies with time, the geometry near the neutral points (points ge in a way that may be considered as the field lines disconnecting ay be argued that in this case, the usual field-line reconnection plicable. As will be shown in II.5 this is not correct. The field ies are erroneous also in this case.

II.4. Filaments

OF FILAMENTS

are often observed in cosmic plasmas. There seems to be a on true filamentary structures to sheet structures, via structures of Consequently, from a phenomenological point of view a clear ugments and sheets is not called for.

ible to *in situ* measurements, there are the following filamentary are observed to be associated with, or are likely to be associated

filaments parallel to the magnetic field are very often observed gure II.3). They are sometimes very thin, with thickness down to under conditions that suggest that they are due to *Birkeland cur- in situ* measurements have not yet completely clarified the relation ctures and the electric currents. This also holds for the often very *traperies*. The *auroral electrojet* itself is of a filamentary character. no doubt that it carries a current.

nts and the *in situ* measurements of strong electric fields in the especially at heights of one Earth radius above the surface, denson- filamentary structures. These structures, which often have elliptical ions are likely to be produced by Birkeland currents. re of Venus, 'flux ropes' are observed with a structure which show at they are produced by filamentary currents. Their diameters are A.7).

re not accessible to *in situ* measurements, we often observe fil- prominences, spicules, coronal streamers, polar plumes, etc. (see In all these cases there are convincing arguments for

CHAPTER II

17



Fig. II.3. Auroral rays in a corona. This pencil sketch by Nansen (in December 1894) gives a better picture of the filamentary structure than photographs, because of the long exposure time needed compared with the fluctuations in the auroral rays.

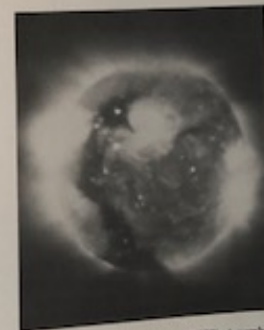


Fig. II.4. Soft X-ray photograph of the Sun from Skylab (1973). A number of loops are seen on the disc which are identified with high density regions. The looplike structures may be caused by electric currents. (American Science and Engineering)

Structure Formation of Universe

- Gravitational : Well known
- Plasma-mediated: Not yet well known

e.g. AGN (prior to becoming a Galaxy) with plasma as the disk, or formation of cluster of AGNs.
even stellar formation out of plasma.

e.g. collaboration of gravity and plasma

(plasma ← **amorphous**, and thus anti-structure entity in blood, as well as in ionized gas)

But!



plasma + B : provides **texture** to weave the structure
of the Universe on (many examples in textbook)

Structures in Universe

- Interplay of **gravity** and **B**

Examples:

- **Stellar dynamics**
(see: NB)
- **AGN disk dynamic**

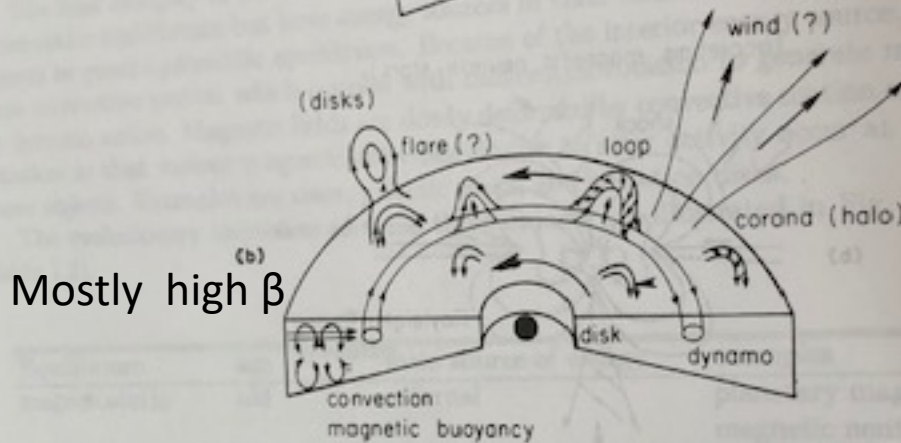
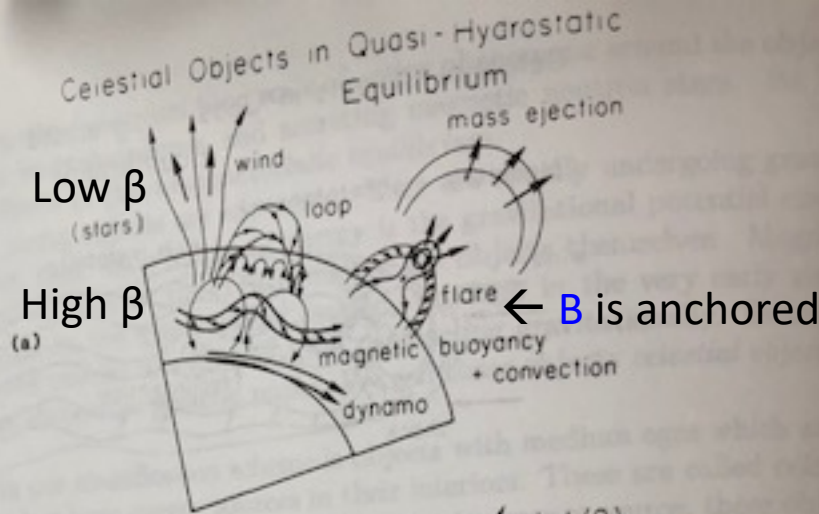
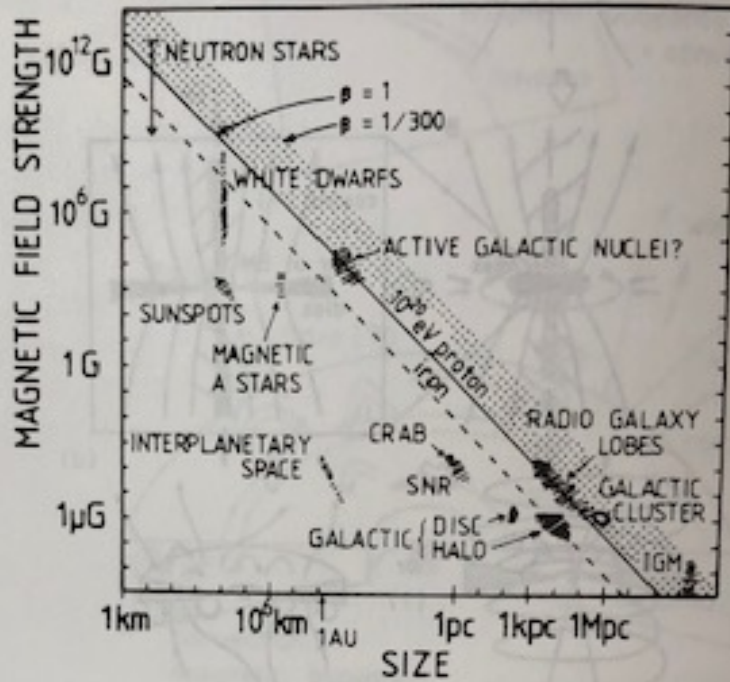


FIGURE 1.8 The structure of objects in quasi-hydrostatic equilibrium.

	ideal or nonideal MHD	steady	nonsteady
low β region	nonideal MHD	corona	flare
	ideal MHD	wind	mass ejection (jet)
high β region		magnetic structure	
		magnetoconvection	
		magnetic buoyancy	
		↑ dynamo	
		↑ differential rotation	

Magnetic fields and astrophysical objects:



Magnetic field **B** vs size of objects

10 Magnetic field strength of various celestial objects as a function of their sizes (fr

On the other hand, an example of quasi-steady release of magnetic energy is the solar wind. If the loop is open to interplanetary space, a wind is created. Although there are many uncertainties in the disks (especially in the inner disk), one possibility is that the disk has a structure similar to the solar wind as illustrated in Fig. 1.8b.

Fundamental Processes in Objects in Non-Equilibrium

A prototype of these objects is the *star forming region*, we will study the physics of star forming regions (Fig. 1.9). (The same basic physics is involved in the formation of galaxies.) In the first stage of gravitational contraction of

Globally,
 $B \sim 1/\lambda$
 why?

NB:

current tube-current tube interaction

Tube coalescence (and reconnection)

Flux twist and untwist

pp.220-221

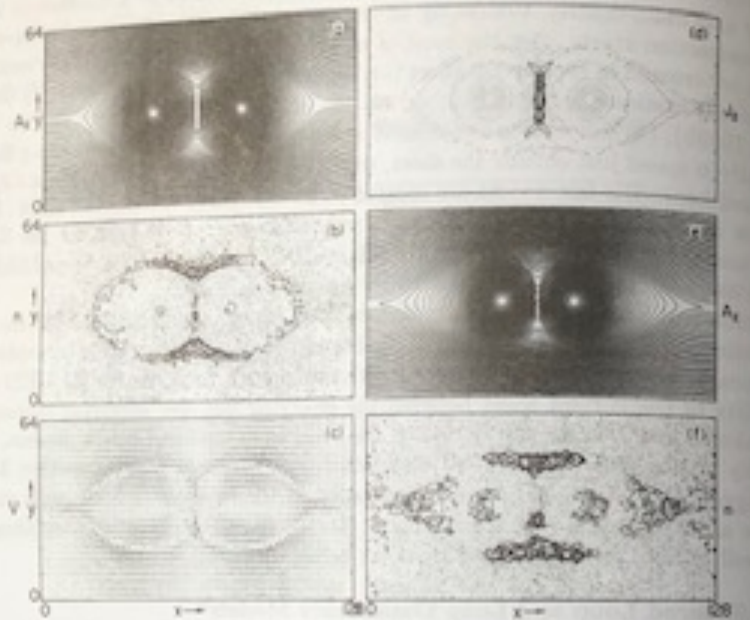
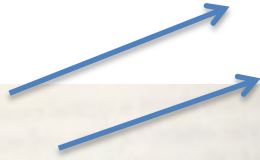


FIGURE 3.57a Spatial pattern of various physical quantities before and during explosive coalescence (from Tajima *et al.*, 1983).

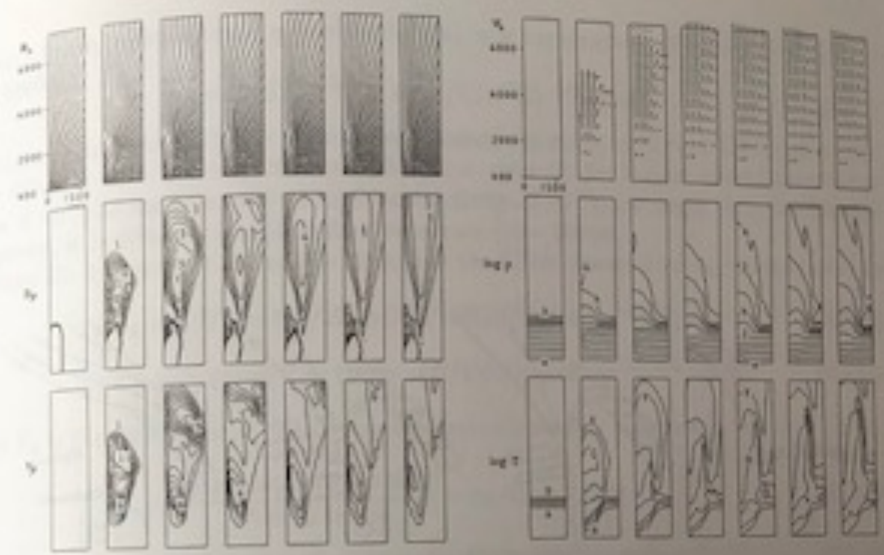
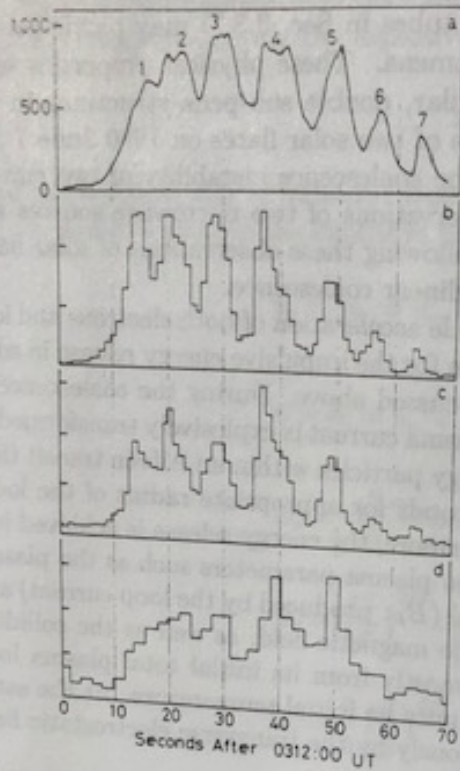
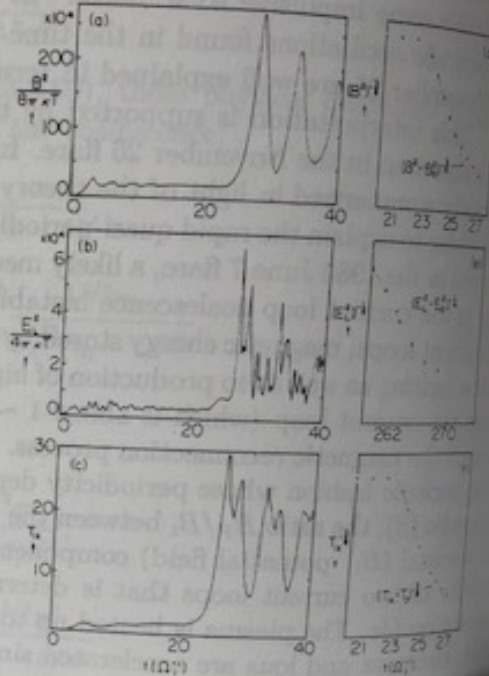


FIGURE 3.57b The unwinding magnetic-twist-jet model by Shibata and Uchida (1985a). These figures show the results of a 2.5D axisymmetric MHD numerical simulations of the dynamical relaxation of a nonlinear magnetic twist in the upper chromosphere; from the top to the bottom in the left column, the poloidal field lines (B_p), the toroidal field (B_t), and the azimuthal (rotational) velocity (V_ϕ) contours; in the right column, the velocity vectors (V), the density ($\log \rho$) and the temperature ($\log T$) contours in a logarithmic scale. The horizontal and vertical sizes of the computing box are 1600 km and 7000 km, respectively. Times are in units of seconds, and the maximum velocity of the jet is about 400 km s^{-1} . The scale of the velocity vector is shown above the frame of $t = 0$ of V . The contour level step width for $\log \rho$ and $\log T$ is 0.5. Note that the jet spins about the z -axis with a rotation velocity of $\sim 60 \sim 200 \text{ km s}^{-1}$. Note also that a jet appears and propagates just ahead of the dense

Flare eruption observed



Simulated eruption of flux tubes



NB:

Solar flare eruption

(example of stellar dynamics)

Coalescence of current tubes

Explosive coalescence (and reconnection)

low β

(no toroidal field)

FIGURE 3.63 Current loop coalescence model of flares by Tajima *et al.* (1987). These figures show the explosive increase of field energies and temperature during the coalescence of two magnetic islands, based on the electromagnetic particle simulations. Note that the magnetic energy, $\sim B^2$, the electrostatic energy, $\sim E^2$, and the temperature, T , diverge as $(t_0 - t)^{-8/3}$, $(t_0 - t)^{-4}$, $(t_0 - t)^{8/3}$, respectively. Note also the vigorous, large amplitude oscillations of these quantities just after the explosive phase (Tajima *et al.*, 1987). Electromagnetic signals observed from the June 7 flare Tajima *et al.*, 1987).

coincides with the peak of the corresponding γ -ray pulse [Fig. 3.63(j)] and with the small hump in hard X-ray time profiles.

3. The starting times of hard X-rays, prompt γ -ray lines, and microwaves coincide within ± 2.2 seconds. Therefore, the acceleration of electrons (up to several MeV) and ions (up to several tens of MeV/nucleon) must have begun almost simultaneously. The time scales of the accelerations are less than 4 seconds.
4. The height of the microwave source was estimated to be ...

Examples of base processes

Parker instability

(ballooning instability) → Flux buoyancy

MRI → twisted magnetic amplification; jet formation

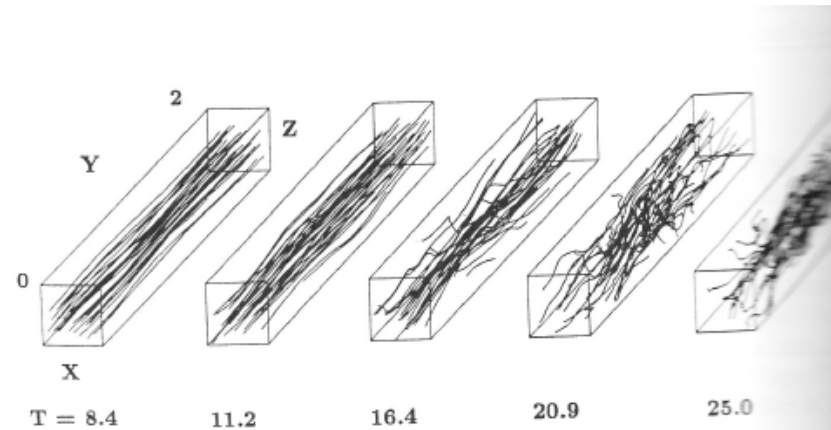
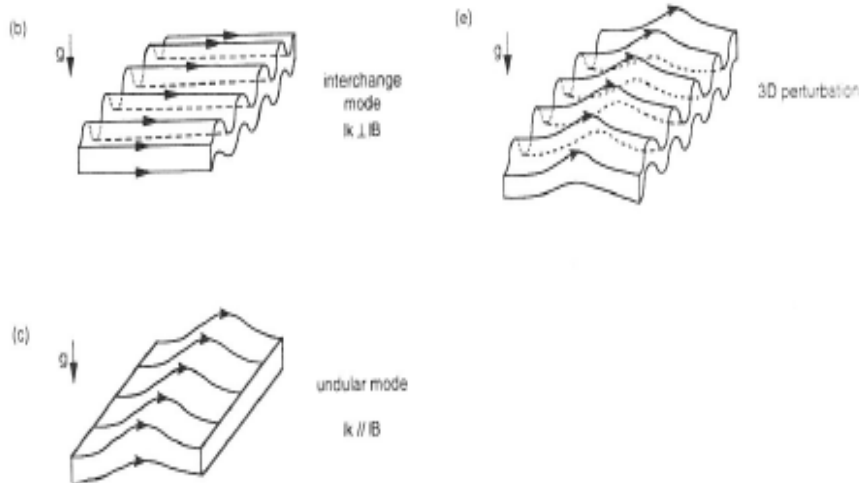


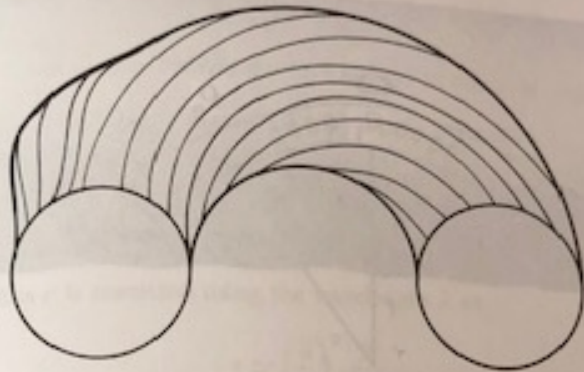
FIGURE 3.18 Interchange mode and undular (Parker) mode of magnetic buoyancy instability.

FIGURE 4.27 Magnetic field lines for model T in the eigenmode growth state [$t = (8.4 - 16.4)/\Omega$] saturation stage [$t = (20.9 - 25.0)/\Omega$] (Matsumoto and Tajima, 1995).

3.2.1.2 Magnetic Buoyancy Instability and Parker Instability

4.2.3.6 Effects of the Parker Instability*

When the vertical gravity is included, magnetic field escapes from the disk due to the Parker instability (the magneto-buoyancy instability; see Sec. 3.2). The growth rate of the Parker instability is $2 - 5H/v_A$, the growth rate of the Parker instability becomes comparable to that of the magnetic shearing instability as β approaches



Similar to the ballooning mode

FIGURE 3.19 Ballooning instability in a magnetically confined torus plasma (e.g., Tokamak). Major radius (R) and minor radius (a) of a torus are shown.

3.2.2 Parker Instability

3.2.2.1 Critical Wavelength

The Parker instability occurs when magnetic fields are disturbed to undulate. Hence the magnetic tension force acts as a stabilizing force. Only when the buoyancy force becomes larger than the magnetic tension force, the Parker instability occurs;

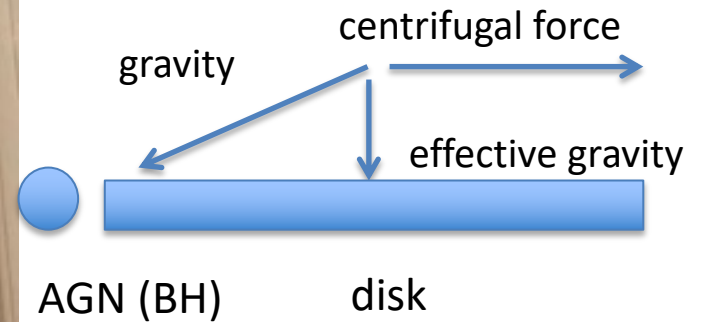
$$\Delta\rho g > \frac{B^2}{4\pi r}, \quad (3.2.32)$$

where r is the curvature radius of the field line.

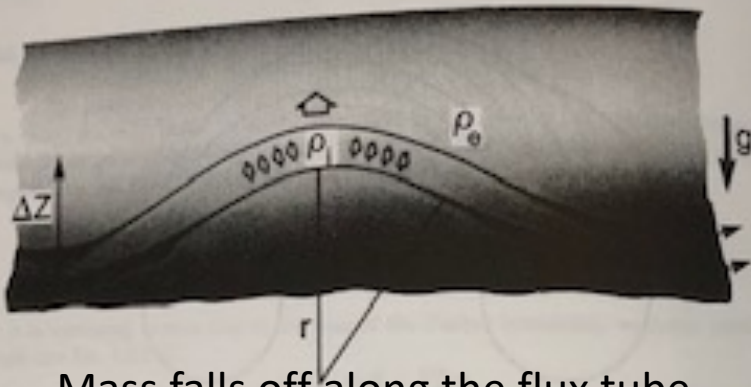
Consider an isolated flux tube embedded in a field-free medium, undulating with a wavelength λ along the flux tube. In this case, magnetic buoyancy force is given by

$$\Delta\rho g = \frac{B^2}{8\pi H}, \quad (3.2.33)$$

Parker Instability



Nonlinear evolution of Parker Instability



Mass falls off along the flux tube
 → Stimulate further growth of balloon
 → "overshoot"

FIGURE 3.20 Undulating flux tube (or sheet).

as shown before (Eq. 3.2.4). Since the magnetic tension force is of order of $B^2/(4\pi\lambda)$, the instability condition becomes

$$\lambda > 2H. \quad (3.2.34)$$

Consequently, there is a critical wavelength below which the Parker mode is stable and the critical wavelength is of order of the local pressure scale height. As discussed earlier, above isothermal isolated flux tube is not in equilibrium, and hence these calculations are not exact (buoyancy force is too large).

Now consider a flux sheet in equilibrium and assume that both sound speed C_s and Alfvén speed V_A are constant. The unperturbed state of plasmas and magnetic field are given by the following equations,

$$p/p_0 = \rho/\rho_0 = B^2/B_0^2 = \exp(-z/\Lambda), \quad (3.2.35)$$

where

$$(3.2.36)$$

obtained from a hydrostatic balance along the flux tube (sheet) and there is no magnetic force along the flux tube, the density at the top of the raised portion of the tube becomes

$$\rho_e(\Delta z) \approx \rho_0 \exp(-\Delta z/H) \approx \rho_0(1 - \Delta z/H), \quad (3.2.37)$$

where

$$H = C_s^2/g. \quad (3.2.38)$$

On the other hand, the density outside the tube (sheet) at the same height (Δz) is

$$\rho_o(\Delta z) \approx \rho_0 \exp(-\Delta z/\Lambda) \approx \rho_0(1 - \Delta z/\Lambda). \quad (3.2.39)$$

Hence, the net density depression at the top of the loop is

$$\Delta\rho \approx \rho_e(\Delta z) - \rho_o(\Delta z) \approx \rho_0\Delta z\left(\frac{1}{H} - \frac{1}{\Lambda}\right). \quad (3.2.40)$$

The curvature radius r is rewritten using the wavelength λ as

$$r \approx \left(\frac{\lambda}{4}\right)^2 \frac{2}{\Delta z}. \quad (3.2.41)$$

Then after some manipulation, the condition for occurrence of the Parker instability $\Delta\rho g > B^2/4\pi r$ becomes

$$\lambda^2 > \lambda_c^2 = 16\Lambda^2/(1 + 1/\beta), \quad (3.2.42)$$

where β is the ratio of gas pressure to magnetic pressure.

Finally the instability condition for wavelength becomes

$$\lambda > \lambda_c = 4\Lambda/(1 + 1/\beta)^{1/2}. \quad (3.2.43)$$

An exact treatment (Parker, 1966, 1979) shows the dispersion relation for $k_\perp\Lambda \gg 1$ as follows

$$(2/\beta + \gamma)\Omega^4 + [(4/\beta)(1/\beta + \gamma)(k_\perp^2\Lambda^2 + 1/4) + \gamma - 1]\Omega^2 + (2/\beta)k_\perp^2\Lambda^2[(2/\beta)\gamma k_\perp^2\Lambda^2 - (1 + 1/\beta)(1 + 1/\beta - \gamma)] = 0, \quad (3.2.44)$$

where

$$\Omega = \frac{\omega\Lambda}{C_s} \quad (3.2.45)$$

and y is the direction perpendicular to both vertical and magnetic fields. From this, we find the exact critical wavelength for $k_\perp\Lambda \gg 1, \gamma = 1$ as

Magnetic buoyancy (simple derivation)

Pressure equilibrium: $\rho_i = \rho_e - B^2 / 8\pi H$, where the scale height $H = T / Mg$

Buoyancy force: $\Delta\rho g = B^2 / 8\pi H$

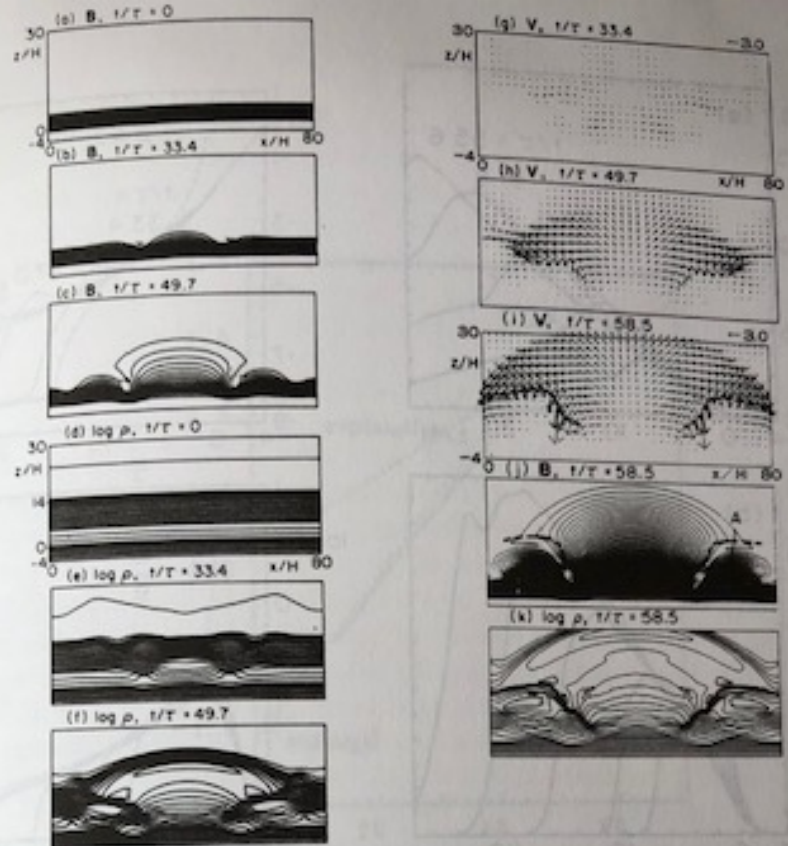
The Parker **instability**: $\Delta\rho g > B^2 / 4\pi r$, where r the tube curvature

The unstable wavelength for Parker: $\lambda > 9H$ when $\beta \gg 1$

Loop brightening

Further nonlinear manifestation of Parker process

Feet of the flux loop emit EM signals by bombardment of plasma to the disk surface



The nonlinear simulation results of the Parker instability triggered by the localized perturbation in Fig. 3.30. (a) The magnetic field lines $\mathbf{B} = (B_x, B_z)$, (b) the velocity vector $\mathbf{V} = (V_x, V_z)$ ($\log \rho$). Note that the magnetic flux expands approximately self-similarly (from Shibata et al.

active-Parker instability (Nozawa et al., 1992) and in the 3D Parker interchange mode (Matsumoto et al., 1993; see Sec. 3.2.2). Find that the Alfvén speed in the rising loop increases with height. This means that the plasma β decreases with height and explains why we have a low β coronal plasma. As magnetic loop expands, it tends to be current free since both the buoyancy and drag forces become smaller than the magnetic force as the loop rises (see e.g. (3.2.81).

Shibata et al. (1989a) found these results assuming isolated magnetic flux tubes; the same results are found also by assuming continuous magnetic field (Shibata et al., 1996).

Magnetic buoyancy and twist in **jets** from accretion disk

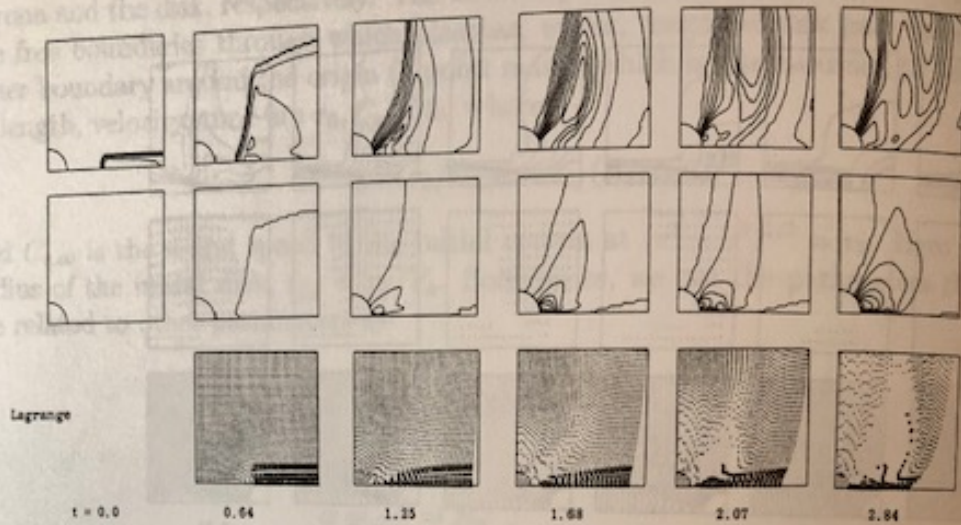


FIGURE 4.53 2.5D MHD sim. of magnetic twist jet (Shibata and Uchida, 1986a): v_ϕ , B_ϕ , Lagrange.

of jet.

Figure 4.55 shows the dependence on the plasma β . It is seen that the magnetic field is more rigid in low β ($= 0.3$) case, while it is more undulating in high β ($= 5$) case. It is found that the velocity of jet is higher in low β case than in high β case. Empirical relation is written as

$$V_{\text{jet}} \sim \beta^{-0.3 \sim -0.4} \sim B^{0.5 \sim 0.7}.$$

Interestingly, this relation is roughly in agreement with the relation of Michel's minimum energy solution for a fast rotator (equation (4.3.35) in previous subsection). According to Shibata (1986, unpublished), the low β jet is accelerated mainly by the centrifugal force, whereas the high β jet is by the magnetic pressure gradient force. The dependence of jet velocity on initial rotational velocity is shown in Figure 4.56. From this, we find that even in the Keplerian case leads to contraction due to magnetic braking and hence eventually to a slower velocity of the jet is slower than the sub-Keplerian case. More detailed comparison between the jet formation and the Balbus-Hawley mechanism (or Velikhov-Chandrasekhar)

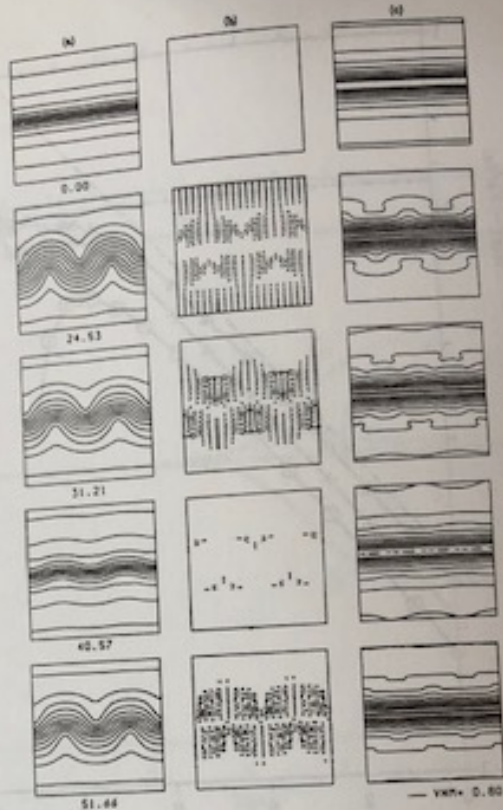
A consequence of Parker process

Beginning of structure formation

via Parker process

Consequences:

- 1. the **escape** of amplified B-field in the disk
2. pinching of plasma radially accentuated, forming **streaks** of dense regions
3. allow accentuated **magneto-rotational instability onset**
4. assist **jet formation**
5. assist **accretion of clumped matter**



3.27 Nonlinear evolution of the Parker instability in the case of weak magnetic field ($\beta = 0.88$). Note that in this case shock waves are not formed, but the nonlinear oscillation occurs

$H_m = C_s^2/g_{max}$ and $g_{max} = 0.385GM/r_0^2$. When applying this result on disks and galaxies, we can assume H_m approximately corresponds to the disk when $\beta > 1$. This result would be important to estimate the accretion loops produced by the Parker instability in accretion disks and in

5 Self-Similar Evolution*

et al. (1989a, 1989b) found a self-similar expansion of a magnetic loop in the case of the Parker instability. They performed 2D nonlinear simulations of an isolated magnetic flux sheet embedded in a field free gas to explain the emergence of magnetic flux tubes in the solar atmosphere. The point of their model is that the magnetic field in the solar region